Materials Science and Engineering C 55 (2015) 482–489

Contents lists available at ScienceDirect

Materials Science and Engineering C

journal homepage: www.elsevier.com/locate/msec

# Curcumin-reduced graphene oxide sheets and their effects on human breast cancer cells

Shadie Hatamie [a], Omid Akhavan [b,c,*], Sayed Khatiboleslam Sadrnezhaad [a,c], Mohammad Mahdi Ahadian [c], Mandar M. Shirolkar [d], Haiqian Q. Wang [d]

[a] Department of Materials Science and Engineering, Sharif University of Technology, Tehran, Iran
[b] Department of Physics, Sharif University of Technology, P.O. Box 11155-9161, Tehran, Iran
[c] Institute for Nanoscience and Nanotechnology, Sharif University of Technology, P.O. Box 14588-89694, Tehran, Iran
[d] USTC-SHINCRON Joint Laboratory, Hefei National Laboratory for Physical Sciences at the Microscale, University of Science and Technology of China, Hefei, Anhui 230026, China

ARTICLE INFO

*Article history:*
Received 17 November 2014
Received in revised form 11 May 2015
Accepted 28 May 2015
Available online 31 May 2015

*Keywords:*
Graphene
Curcumin
Cell viability
Cancer cells

ABSTRACT

Curcumin (as a natural reductant material) was utilized for green reduction and functionalization of chemically exfoliated graphene oxide (GO) sheets. The π–π attachment of the curcumin molecules onto the curcumin-reduced graphene oxide (rGO) sheets was confirmed by Raman and Fourier transform infrared spectroscopies. Zeta potential of the GO sheets decreased from about −40 mV to −20 mV, after the green reduction and functionalization. The probable cytotoxicity of the curcumin-rGO sheets was studied through their interactions with two human breast cancer cell lines (MDA-MB-231 and SKBR3 cell lines) and a normal cell line (mouse fibroblast L929 cell line). The curcumin-rGO sheet with concentrations <70 μg/mL in the cell culture medium, not only exhibited no significant toxicity and/or cell morphological changes, but also caused some cell growths (~25% after 48 h incubation time). Nevertheless, at 70 μg/mL, initiation of some cell morphological changes was observed. At higher concentrations (e.g., 100 μg/mL), some slight cytotoxic effects (resulting in ~15 − 25% cell destruction) were detected by MTT assay. In addition, the interaction of the rGO sheets and cells resulted in apoptosis as well as morphological transformation of the cells (from elongated to roundup morphology). These results indicated the concentration-dependent toxicity of functionalized-rGO nanomaterials (here, curcumin-rGO) at the threshold concentration of ~100 μg/mL.



## 1. Introduction

Graphene, as one of the most promising nanomaterials in upcoming nanotechnology-based bioapplications [1], has attracted many attentions in recent years. In this regard, it efficiently utilized in bactericidal [2–6], antiviral [7] and nematocidal [8] purposes and applied in disease diagnosis [9], extremely sensitive biosensing [10–12], stem cell-based tissue engineering [13–15] as well as neural cell proliferation, differentiation and network regenerations [16–19], drug delivery [20,21], and cancer cell imaging, targeting as well as therapy [22–25].

Due to potential cyto- and geno-toxicity of graphene, even at low concentrations (~10 μg/mL) [26,27], further attentions and treatments are required in bioapplications of graphene, especially in drug delivery and cancer therapeutic applications which usually require high concentrations of graphene (typically >10 μg/mL) [28–30]. Recently, it was shown that functionalized graphene sheets can exhibit lower cytotoxic effects [31–33]. Moreover, it was found that some green reductants having aromatic structures, such as vitamin C [34], melatonin [35,36], polyphenols of green tea [37,38] and ginseng [32], can not only reduce graphene oxide (GO) sheets, but also functionalize the reduced graphene oxide (rGO) ones through π–π attachment of the reductant molecules onto the rGO surface. Recently, it was found that green tea polyphenol-functionalized rGO sheets can also decrease the reactive oxygen species (ROS) generated in cell culture media, while hydrazine-rGO sheets induce more ROS generation [39].

Among the natural reducing agents, curcumin (as the main component and coloring agent in the rhizomes of curcuma longa (zingiberaceae)) is known as one of the effective natural antioxidants. For example, it has successfully been utilized in many therapeutic applications as antioxidant, anti-inflammatory, and anticancer agent [40,41]. There are also some recent reports concerning application of curcumin in synthesis and functionalization of nanoparticles having antioxidant properties [42]. But, so far, no investigation has been reported about synthesis and functionalization of rGO sheets by curcumin.

In this work, at first, curcumin was utilized for simultaneous reduction of chemically exfoliated GO sheets and functionalization of the rGO ones. The π–π attachment of the curcumin molecules onto the rGO sheets was studied by Raman and Fourier transform infrared (FTIR)

* Corresponding author at: Department of Physics, Sharif University of Technology, P.O. Box 11155-9161, Tehran, Iran.
*E-mail address:* oakhavan@sharif.edu (O. Akhavan).

http://dx.doi.org/10.1016/j.msec.2015.05.077
0928-4931/

spectroscopies. Then, the potential concentration-dependent cytotoxicity of the curcumin-functionalized rGO sheets (with concentrations up to 100 μg/mL) was investigated against two human breast cancer cell lines and a normal mouse cell line using MTT assay and monitoring the cell morphological changes.

## 2. Experimental

### 2.1. Synthesis of GO

Graphite oxide was synthesized by using a modified Hummer's method, as its details reported previously [43]. In summary, 0.5 g graphite powder (≤20 μm, Fluka) was added into 23 mL sulfuric acid (98%, Merck) in an ice bath. Then, 0.5 g $KMnO_4$ was gradually added into the mixture and stirred with for 10 min. After that, 2 g $NaNO_3$ was added into the solution and stirred again for 3 h at 35 °C. The obtained solution was diluted by adding 40 mL deionized (DI) water. The reaction in the solution was over by adding a clear solution of DI water and $H_2O_2$ (30%). The obtained graphite oxide suspension (with a light yellow color) was washed with diluted HCl (with a volume ratio of 1:10 for HCl to DI water) to remove the residual ions. Finally, the materials of the suspension were filtered using a filter paper and washed with DI water for several times till pH of the aqueous graphite oxide suspension (with a brown color) reached to ~5. Then, the graphite oxide suspension was sonicated at a frequency of 100 kHz with power of 120 W for 40 min to exfoliate the graphite oxide to GO sheets. Then, the sonicated suspension was centrifuged at 3500 rpm for 30 min to remove the unexfoliated materials.

### 2.2. Reduction of GO by curcumin

For the reduction of the GO suspension, 5 mg curcumin (1,7-bis[4-hydroxy-3-methoxyphenyl]-1,6-heptadiene-3,5-dione) was dissolved in the 10 mL ethanol to obtain a uniform yellowish solution. Then, the curcumin solution was gradually added into the homogeneous GO suspension, while it was stirred. Then, 10 μL of ammonia solution was added into the curcumin-GO suspension in order to increase its pH to 10. This resulted in better stability and homogeneity of the curcumin-GO suspension. The suspension was heated at 85 °C for 120 min. Finally, the obtained curcumin-rGO suspension (with black color) was dialyzed by using a dialysis pack and centrifuged at 3000 rpm for 20 min to remove any residuals (especially the ammonia) and control the pH ~7.

### 2.3. Material characterization

The sheet-like morphology of the curcumin-rGO sheets was examined by transmission electron microscopy (TEM). For sample preparation, at first, the rGO sheets were dispersed in ethanol and a drop of sample was placed on a copper grid coated with a carbon film. Then, the loaded grid was dried in air at room temperature. The surface topography and height profile of the graphene sheets were studied by atomic force microscopy (AFM, Digital Instruments NanoScope V) in tapping

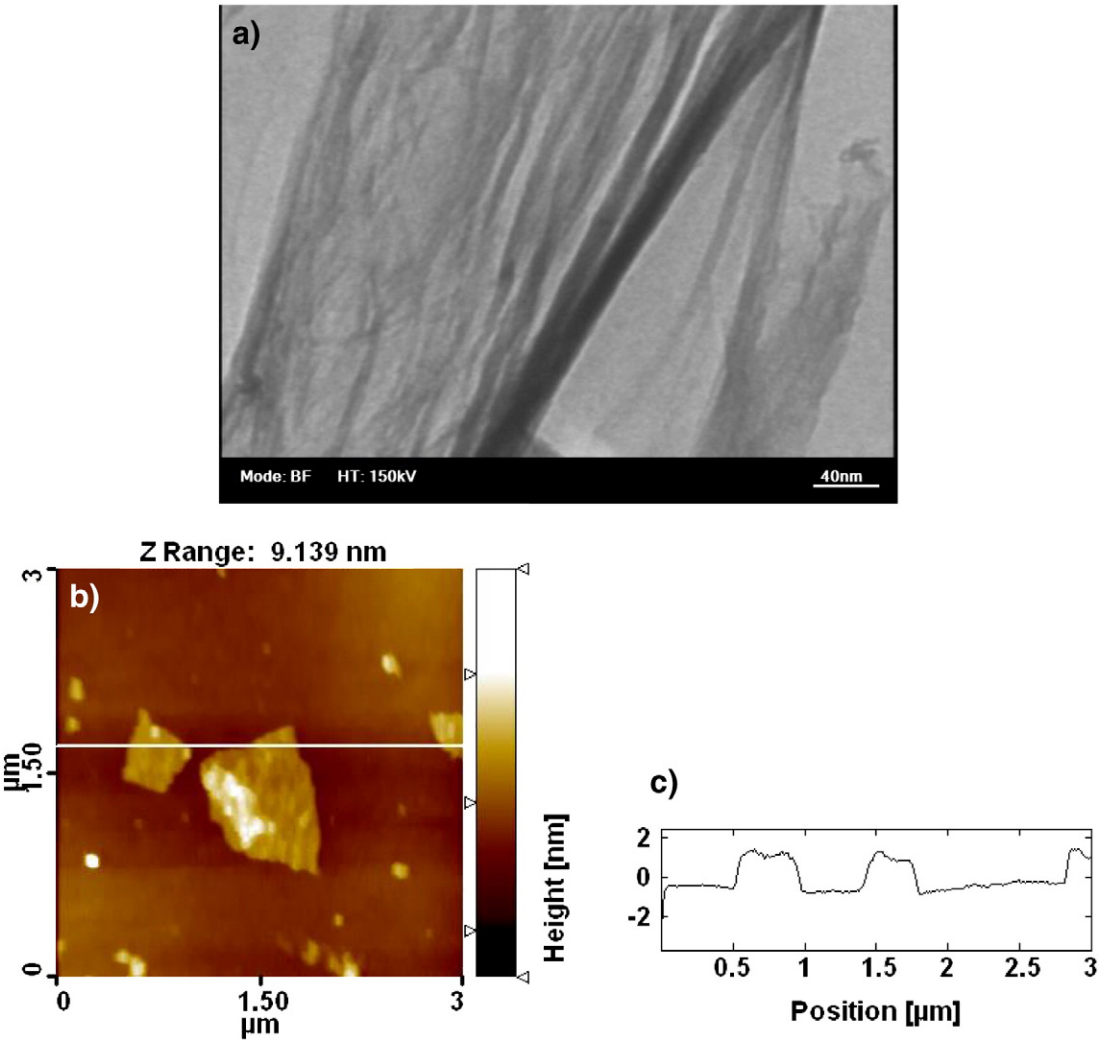


**Fig. 1.** a) TEM and b) AFM images of curcumin-rGO sheets. (c) shows height profile diagram of the rGO sheets marked by a line in (a).

mode. The samples for AFM imaging were prepared by drop-casting a diluted graphene suspension (10 μg/mL) onto a cleaned $SiO_2$/Si(100) substrate. Raman spectroscopy (HR-800 Jobin-Yvon) was performed at room temperature using an Nd-YAG laser source operating at a wavelength of 532 nm. The samples for Raman spectroscopy were prepared by drop-casting the graphene suspension onto the cleaned $SiO_2$/Si(100) substrates. UV–vis spectrophotometer (UV-2550 UV–vis SHIMADZU) was utilized to record the absorption spectra of the graphene suspensions. FTIR spectra of the samples were obtained by using an EQUINOX 55, Bruker. The samples were prepared by grinding the graphene powders (obtained through precipitates of the dried suspensions) along with KBr, and compressing into thin pellets. Thermo-gravimetric analysis (TGA) and differential scanning calorimetry (DSC) were performed using a SDT Q600 V8.3 Build 101 system at a ramp rate of 1 °C/min up to 1000 °C in a nitrogen environment with flow of 100 mL/min. X-ray photoelectron spectroscopy (XPS) was applied to analyze the chemical state of carbon atoms in the GO and curcumin-rGO samples. The XPS data were gathered by a hemispherical analyzer supplied by an Al Kα X-ray source working at an energy of 1486.6 eV in a vacuum better than ~$10^{-7}$ Pa. The XPS peaks were calibrated by fixing the Au(4f7/2) corelevels of the samples coated by a thin Au layer (using a desktop sputtering system (Nanostructured Coating Co., Iran)) at 83.7 eV. Then, the XPS peaks were analyzed by deconvolution using suitable Gaussian components after a Shirley background subtraction. X-ray diffraction (XRD) patterns were obtained by using a Philips X'Pert Pro MRD system with $\lambda_{Xray}$ of 1.54 Å. Zeta potential of the rGO sheets dispersed in sodium phosphate buffer (PBS) at pH ~7 was measured by a Malvern Instrument Ltd.-UK.

### 2.4. Cell assays

Viability of the cells exposed to the graphene samples was checked by using MTT assay as a colorimetric and non-radioactive assay. In fact, MTT assay is based on cellular uptake of 3-[4,5-dimethylthiazol-2yl]-2,5-diphenyltetrazoliumbromide (MTT) and subsequently reduction in the mitochondria of living cells into dark blue formazan crystals. MTT viability assay was performed using breast cancer cell lines (MDA-MB-231 and SKBR3) and a mouse fibroblast (L929) cell line (applied as a normal cell) which were prepared from Pasture Institute of Iran. The cancer cells (typically ~$2 \times 10^4$ cells) and L929 normal cells (typically ~$5 \times 10^4$ cells) were grown in 48-well plates and cultured in minimum essential medium Eagle (MEM), supplemented with 10% fetal bovine serum (FBS) and 1% penicillin at 37 °C under 5% $CO_2$ for 24 h followed by washing using serum-free MEM and incubated with different concentrations of graphene. The curcumin-rGO sheets used for viability assay were also put in an autoclave at 120 °C for 20 min. After 48 h incubation, 100 μL of MTT was added into each 48-well plate, followed by 2 h incubation at 37 °C under 5% $CO_2$. Finally, the suspended graphene sheets were removed by centrifuging at ~20,000 rpm for 15 min and then the supernatant was collected. The insoluble formazen, which was produced by live cells, was solubilized in dimethylsulfoxide (DMSO), and then, optical density (OD) of each well was monitored at 570 nm using a micro plate reader (Bio-Tek ELX8000). Meantime, the OD at 655 nm was considered as the reference. The absorbance recorded by a microplate was used for calculation of the survival cells using the following equation:

$$\text{MTT assay(cell viability \%)} = (\text{sample abs 570 nm})/(\text{control abs 570 nm}) \times 100$$

The surface topography and height profile of the MDA-MB-231 cell line and graphene sheets embedded in the cells were studied by AFM in tapping mode. To do this, cleaned $SiO_2$/Si(100) substrates were immersed in 2-well plates containing curcumin-rGO (~10 μg/mL in the culture medium). Then, the substrates were removed from the wells and the breast cancer cells were fixed using glutaraldehyde followed by drying at 37 °C for 20 min.

## 3. Results and discussion

Fig. 1a shows TEM image of one of the curcumin-rGO sheets. It presents the sheet-like morphology of the curcumin-rGO materials with a high transparency (because of their atomic thicknesses). The wrinkles of such thin sheets are also observable in the image.

Fig. 1b presents AFM image of some curcumin-rGO sheets deposited on the $SiO_2$/Si substrate. The height profile diagram of the sheets is also shown in Fig. 1c. It is well-known that the typical thickness of single-layer GO sheets is ~0.8 nm, that is, ~0.44 nm thicker than the typical thickness of graphene (~0.36 nm), due to bonding the oxygen-containing functional groups on each side of GO [44–46]. Fig. 1c shows that thickness of the curcumin-rGO sheets is ~1.5 nm, while our AFM analysis indicated that the average thickness of the synthesized GO sheets was ~0.8 nm (see, for example, [47]). The increase in the thicknesses of the reduced sheets (as compared to the GO ones) was assigned to π–π attachment of curcumin molecules on both sides of the reduced sheets, as previously demonstrated for other aromatic molecules [48], such as ginseng [32], vitamin C [34], melatonin [35], and polyphenols of green tea [37]. AFM, TEM and scanning electron microscopic images of GO sheets were previously reported elsewhere [49,50].

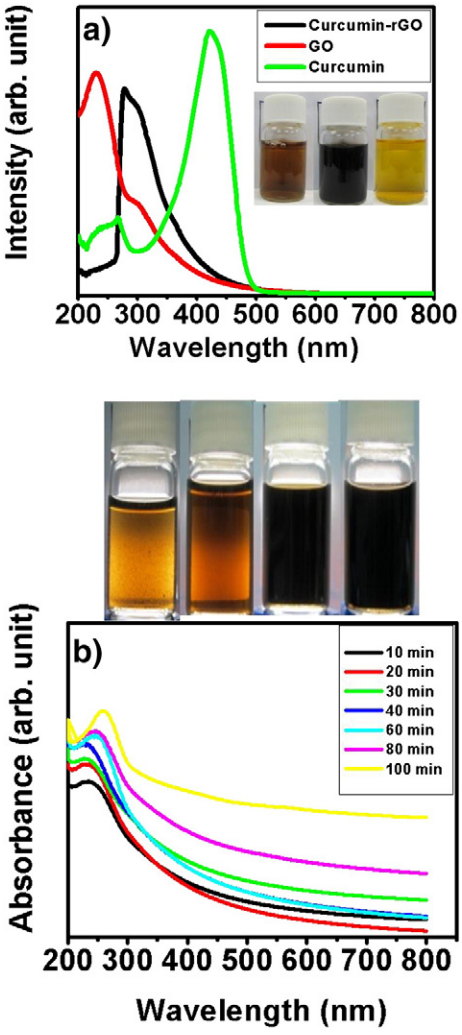


**Fig. 2.** UV–vis absorption spectra of a) GO, curcumin-rGO and curcumin suspensions (0.5 μg/mL) and b) GO suspension (0.1 μg/mL) reduced by curcumin at 85 °C for various periods of time ranging from 10 to 100 min. Digital pictures of a) GO, curcumin-rGO and curcumin suspensions and b) GO suspensions reduced by curcumin at 85 °C for 10, 40, 80 and 120 min (from left to right) are also presented.

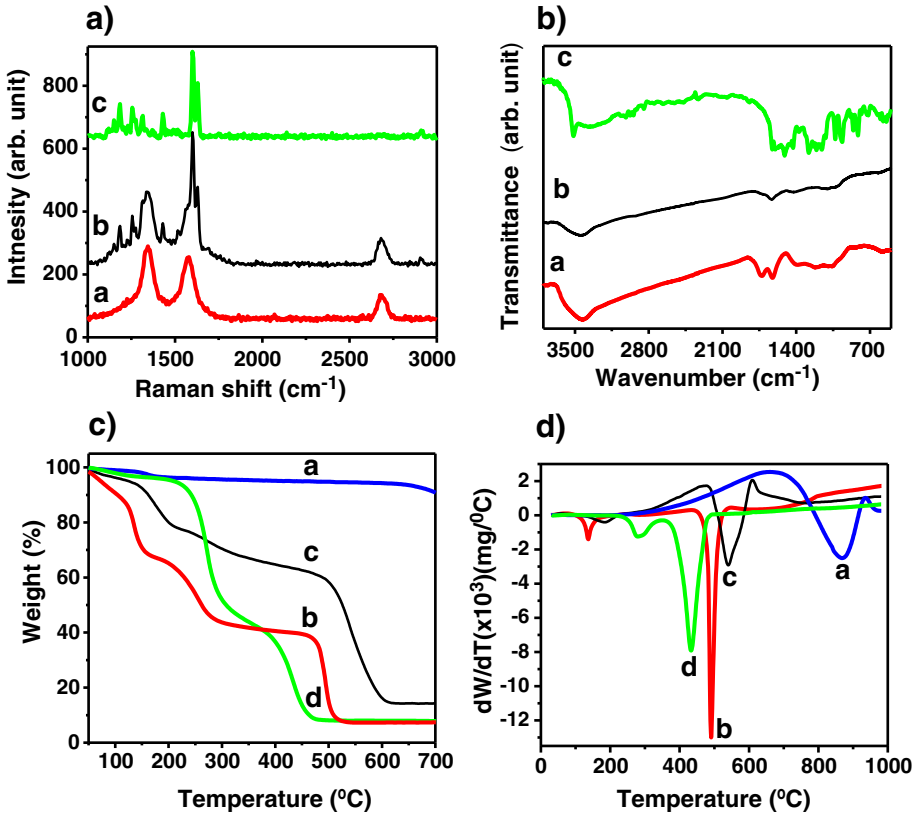


**Fig. 3.** A) Raman and B) FTIR spectra of a) GO, b) curcumin-rGO and c) curcumin, C) TGA curves of a) graphite, b) GO, c) curcumin-rGO and d) curcumin, and D) corresponding mass loss rate (dW/dT) in DSC of a) graphite, b) GO, c) curcumin-rGO, and d) curcumin.

Fig. 2a shows UV–vis absorption spectra of GO and curcumin-rGO aqueous suspensions as compared to the curcumin suspension in ethanol. The GO sample shows an absorption peak at ~230 nm and a shoulder at ~310 nm which are assigned to the π–π transition of C═C and n–π* transition of C═O bonds, respectively [51]. The curcumin spectrum exhibits a strong absorption band at 422 nm and a shoulder at 270 nm, which are consistent with the π–π transition and absorption maxima of the n–π* transition of curcumin in ethanol, respectively [52]. The curcumin-rGO sample exhibits a broad peak at 270 nm, which indicates ~40 nm red-shift relative to the absorption peak of the GO. These changes can be assigned to deoxygenation of the GO sheets. It should be noted that after addition of curcumin into the GO solution, the peak related to curcumin at 420 nm disappeared. This can be assigned to attachment of the chromophore sides of curcumin onto the

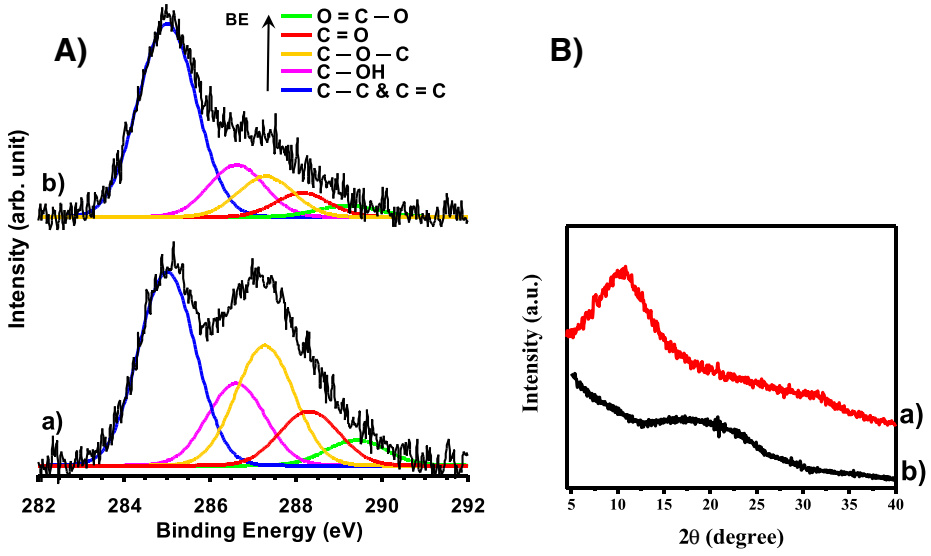


**Fig. 4.** A) Peak deconvolution of C(1s) core level of XPS and B) XRD patterns of a) GO and b) curcumin-rGO samples.

**Table 1**
Zeta potentials of GO and curcumin-rGO sheets with concentration of ~50 μg/mL in PBS with pH ~7.

| Sample | Zeta potential (mV) |
|---|---|
| GO | $-40.1 \pm 0.7$ |
| Curcumin-rGO | $-20.2 \pm 1.13$ |

rGO surfaces [53]. These results indicate reduction of GO by curcumin. The time evolution of reduction is shown in Fig. 2b. This also indicates controllable as well as continuous deoxygenation of GO by curcumin.

Raman spectroscopy is a powerful technique to investigate the carbon structure of graphene materials, especially the ordered and disordered crystal structures and also the single- and multi-layer properties of graphene sheets. Fig. 3A shows Raman spectra of the GO and curcumin-rGO sheets as compared to the spectrum of the curcumin. In Fig. 3A, the typical features of carbon materials, i.e., the G band (~1580 $cm^{-1}$) which is usually attributed to the $E_{2g}$ phonon of the graphitized structure and the D band (~1350 $cm^{-1}$) as a breathing mode of κ-point phonons of $A_{1g}$ symmetry [54,55] associated with local defects/disorder [56,57], are clearly distinguishable. It is known that the peak position of the G band of the single-layer graphene sheets (1585 $cm^{-1}$) shifts about 6 $cm^{-1}$ into lower frequencies after stacking more graphene layers (for 2–6 layers the G band shifts to 1579 $cm^{-1}$) [56–59]. It is also well-established that the 2D band of Raman spectroscopy of graphene materials is much sensitive to stacking of the sheets [60]. For instance, the 2D band of single-layer graphene locates at ~2679 $cm^{-1}$, while for multi-layer graphene (including 2–4 layers), the 2D band appears as a broadened peak with 19 $cm^{-1}$ shift into larger wavenumbers [61]. Furthermore, the $I_{2D}/I_G$ intensity ratio of single-, double-, triple- and multi- (>4) layer graphene is typically >1.6, ~0.8, ~0.30 and ~0.07, respectively (see, e.g., [62–64]). In this work, the peak positions of the G band of the GO and the 2D band of all samples (GO in Fig. 3Aa and curcumin-rGO in Fig. 3Ab) were found at ~1580 and 2680 $cm^{-1}$, respectively. Moreover, the $I_{2D}/I_G$ ratio of the GO was found to be 0.42. These results confirmed that the synthesized GO sheets exhibited multilayer structures with ≤3 single-layer structure, in well consistency with the AFM results. In Fig. 3Ab and Ac, the band located at 2911 $cm^{-1}$ is assigned to the asymmetric stretching vibrations of the $CH_2$ groups of curcumin [65]. The strong bands located at 1630 and 1600 $cm^{-1}$ are attributed to the mixed of C═O and C═C stretching of benzene rings. In addition, the band at 1430 $cm^{-1}$ is assigned to in-plane aromatic C–C–C or C–C–H deformation (in-plane skeletal deformations) [66]. The vibration bands at 1185 and 1150 $cm^{-1}$ are also assigned to bending (connected to keto part) of C–O–C in phenolic part of curcumin molecule [66]. Since similar patterns (in addition to the D, G and 2D bands) are also observable in the spectrum of the curcumin-rGO sample (compare Fig. 3Ab and Ac), it can be concluded that the curcumin molecules were attached on the surface of the rGO sheets.

Reduction of the GO using the polyphenols of curcumin can be further studied by FTIR. Fig. 3B shows FTIR spectra of GO and curcumin-rGO as compared to the spectrum of the curcumin. For the GO, the sharp peak at 1733 $cm^{-1}$ is assigned to the C═O bond of the carboxylic groups. The peak at 1622 $cm^{-1}$ is related to the C═C band [13]. Vibration band of the epoxy is located at 1055 $cm^{-1}$ and O–H sign is appeared at 3386 $cm^{-1}$ [67–69]. After reduction of graphene oxide by curcumin, the vibrational absorption band of carboxylic groups was disappeared (the peak located at the 1733 $cm^{-1}$) and the peak relating to the C–O–C band (at 1052 $cm^{-1}$) became very weak [70]. The FTIR spectrum of curcumin shows the presence of O–H (3514 $cm^{-1}$), C═O and C═C ring (1450–1630 $cm^{-1}$), C–H methyl ring (2845 $cm^{-1}$), aromatic ring (3016 $cm^{-1}$), and C–O–C (1000–1300 $cm^{-1}$) functional groups [71]. By comparing the spectra of the GO and curcumin, it can be concluded that the FTIR spectrum of the curcumin-rGO shows significant reduction of nearly all of the oxygen-containing functional groups especially the carboxylic acid groups and epoxide bonds. Nevertheless, the signatures of curcumin are still observable in the curcumin-rGO sample, indicating attachment of the curcumin molecules on the surface of the reduced sheets.

The functionalization of the rGO by curcumin can be also checked by using TGA and DSC. Fig. 3C and D shows TGA and DSC curves of graphite, GO, curcumin-rGO and curcumin samples. As a benchmark, the raw graphite material exhibited a high thermal stability with only ~10% mass loss up to 700 °C. The GO showed a mass loss of ~20% at around 120 °C due to the water removal, a second mass loss of ~25% at around 200 °C relating to the loss of oxygen-containing functional groups, and a third mass loss of ~30% at around 480 °C due to combustion to carbon dioxide (corresponding to the endothermic DSC signal shown in Fig. 3D). The same TGA trend was also reported previously [72,73]. The curcumin showed only two mass losses at ~280 and 420 °C relating to the removal of the oxygen bonds and combustion, respectively. The curcumin-rGO material exhibited two main steps of mass loss at ~170 and 520 °C due to the water removal and combustion. The slight mass loss at the temperatures >250 °C can be assigned to the removal of the oxygen groups of the residual bonds and/or the curcumin molecules remained on the surface of the reduced sheets. Moreover, the reduced sheets exhibited a higher thermal stability than the GO ones.

To confirm the reduction of GO by curcumin in more details, XPS and XRD techniques were used. Fig. 4A shows XPS peak deconvolution of C(1s) core levels of the GO and curcumin-rGO samples. The peak centered at 285.0 eV was attributed to the C–C and C═C bonds. The other deconvoluted peaks located at the binding energies of 286.6, 287.2, 288.3 and 289.4 eV were assigned to the C–OH, C–O–C, C═O, and

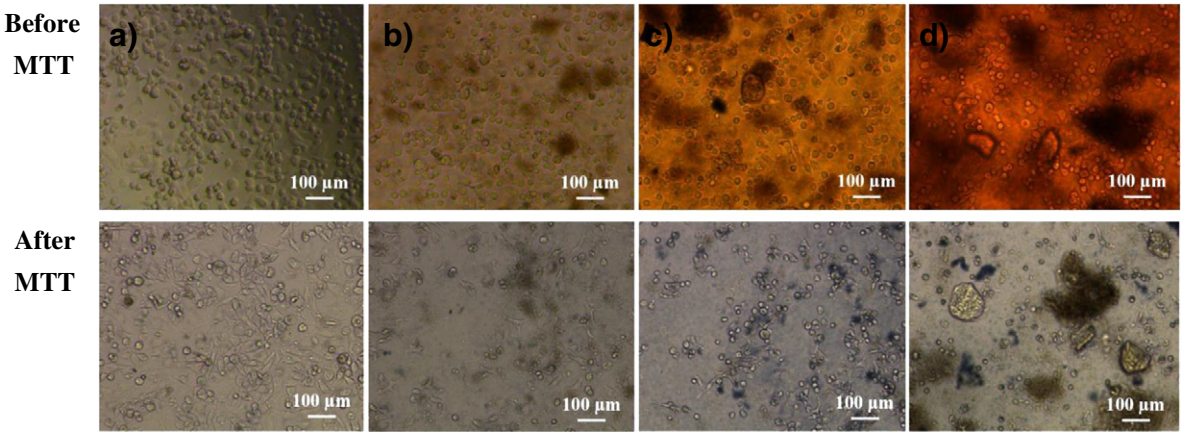


**Fig. 5.** Optical microscopy of breast cancer cell lines SKBR3 incubated with a) 0, b) 10, c) 40, and d) 70 μg/mL curcumin-rGO for 48 h, before and after MTT treatment.

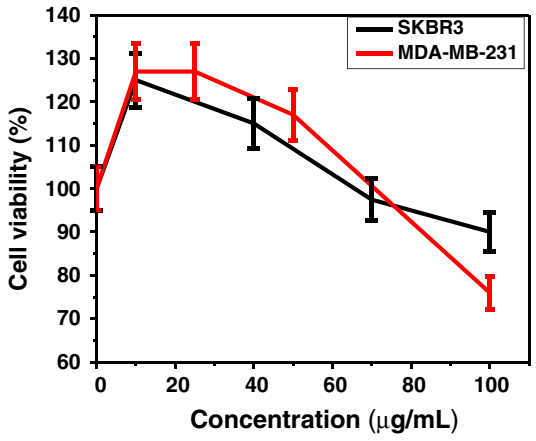


**Fig. 6.** MTT cell viability of a) SKBR3 and b) MDA-MB-230 breast cancer cell lines incubated with curcumin-rGO sheets at various concentrations for 48 h.

O═C–OH oxygen-containing functional groups, respectively (see, e.g., [74,75]). The O/C ratio obtained was 0.52 and 0.37 for the GO and curcumin-rGO samples, respectively. This indicates the effect of curcumin on the deoxygenation of the GO sheets. Moreover, the relative increase in the peak area ratio of the C–OH peak to the C–O–C peak of the curcumin-rGO sample (~88% increase relative to the GO) can be assigned to π–π attaching of the curcumin molecules with phenol groups on the rGO sheets (in consistency with the AFM results).

The crystalline structure of the GO and curcumin-rGO samples was studied by XRD. Fig. 4B presents XRD patterns of the samples. The diffraction peak of exfoliated GO was found at 2θ ~ 11° with crystalline orientation of (002) and interlay space (d-spacing) of ~0.8 nm. For the curcumin-rGO samples, the (002) peak at 2θ ~ 11° disappeared and another reappeared at ~21°, indicating the reduction of the GO sheets and formation of stacked rGO sheets with d-spacing of ~0.4 nm.

Since cell membranes are usually charged, the surface charge of nanomaterials plays a key role in cell–nanomaterial interactions [76]. Zeta potentials of the GO and curcumin-rGO sheets are listed in Table 1. It was found that zeta potential of the GO and curcumin-rGO sheets was negative. The higher zeta potential of the GO sheets than that of the rGO ones can be attributed to the oxygen content of the GO.

To study the cytotoxic effects of curcumin-rGO sheets, the human breast cancer cell lines MDA-MB-231 and SKBR3 were utilized. The optical images of the SKBR3 cells incubated with the curcumin-rGO sheets are shown in Fig. 5. MTT cell viability of the cells exposed to the various concentrations of rGO sheets (ranging from 0 to 100 μg/mL) is also presented in Fig. 6. To monitor the effect of MTT assay on the cells incubated with the rGO, the optical images of the cells after MTT assay were also compared with the images taken before the MTT assay (see Fig. 5). At the concentrations <70 μg/mL, no significant toxic effects was observed. Instead, some cell growth was found, indicating no toxicity of the curcumin-rGO sheets up to this concentration. This biocompatibility can be assigned to scavenging the ROS generated in the culture medium by the curcumin molecules attached onto the rGO sheets, as recently demonstrated for green tea polyphenol-functionalized rGO sheets [39]. The optical images (Fig. 5) show that at 70 μg/mL, the morphology of the cells significantly changed. Consistently, at the higher concentration (100 μg/mL), some more toxic effects (~15 — 25% cell destruction) were detected by MTT assay (Fig. 6). These results indicate concentration-dependent toxicity of functionalized-rGO nanomaterials (here, curcumin-rGO) at the threshold concentration of 100 μg/mL, as also reported previously for other functionalized rGO sheets [31–33].

To have a control sample, the effects of GO (as the starting nanomaterial) on the cancer cells were also checked. It was found that the GO and curcumin-rGO samples exhibit the same time- and concentration-dependent activity. It should be noted that the rGO samples (e.g., hydrazine-rGO ones) usually present higher cytotoxic effects than GO ones, due to generation of more reactive oxygen species, sharper edges [2,26] and/or capability of aggregation resulting in wrapping the cells [36]. Hence, the slight cytotoxic effects of the curcumin-rGO sheets can be assigned to the presence of the curcumin molecules (which contain phenol groups) on the surface of the reduced sheets. The presence of curcumin on the surface of the reduced sheets prevented aggregation of the reduced sheets (i.e., no wrapping the cells) and increase the effective thickness of the sheets (i.e., lower effective interactions of the sharp edges of the sheets with the cell wall membranes).

The time- and concentration-dependent cytotoxic effects of the curcumin-rGO sheets were also checked on L929 cell line as a normal cell. No cytotoxic effects were observed after 24 h incubation time, independent from the concentration of curcumin-rGO. After 48 h, only the concentration of 100 μg/mL could induce a slight cytotoxicity (~10% decrease in the cell viability). However, after 72 h incubation, some more cytotoxic effects were observed, especially at the high concentration of 100 μg/mL (~25% decrease in viability of the initial cells). Hence, the effects of the curcumin-rGO sheets on the cancer cells were also checked after the longer incubation time of 72 h. But, no significant changes were found in the cytotoxic effects of the sheets on the cancer cells after 72 h (as compared to their effects after 48 h). These results confirmed that the curcumin-rGO sheets finally showed the same cytotoxic effects on the cancerous and normal cells, although their effect on the cancer cells is accelerated. The fast interaction of curcumin-rGO sheets with

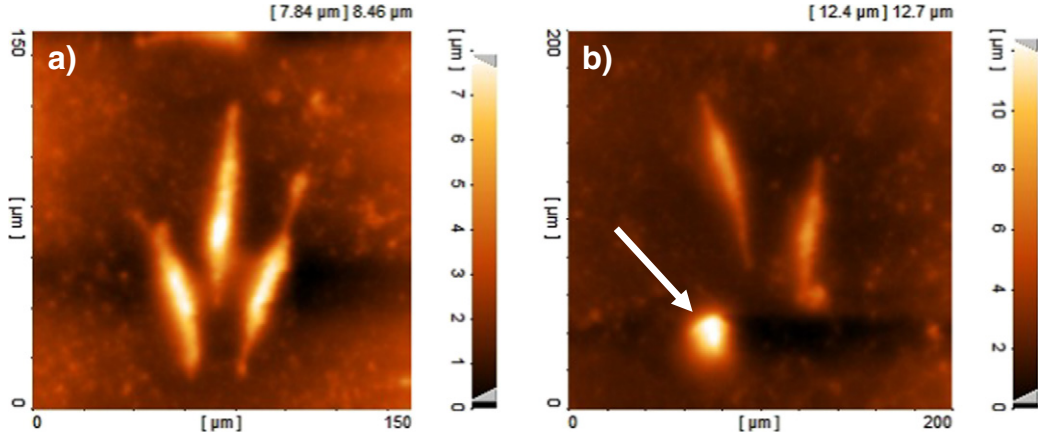


**Fig. 7.** AFM image of MDA-MB-231 cells a) before and b) after exposing to ~100 μg/mL curcumin-rGO sheets for 48 h. The roundup morphology of a dead cell is clearly observable in (b).

the cancerous cells (as compared to normal cells) is consistent with the recent potential applications of functionalized graphene nanomaterials in tumor imaging [77] and cancer therapy [23].

Fig. 7 shows the effect of curcumin-rGO sheets on morphology of MDA-MB-231 cell lines. It was found that by increasing the rGO concentration to ~100 μg/mL, the cell morphology significantly changed. In fact, the cells were roundup and detached from the culture plate after 48 h incubation, as shown in Fig. 7. This can be assigned to apoptosis of the cells effectively interacted by the graphene sheets at such high concentration. Using a statistical analysis for AFM images (~10 images), it was found that ~30% of cell apoptosis occurred after interactions of the cells with curcumin-rGO sheets at a concentration of ~100 μg/mL. This is well consistent with the results obtained by MTT assay. Therefore, we concluded that nearly all the cells inactivated by the curcumin-rGO sheets experienced apoptosis (using AFM and MTT assay).

## 4. Conclusions

Chemically exfoliated GO sheets were successfully reduced and functionalized by curcumin, as a natural reductant material. The π–π attachment of the curcumin molecules onto the rGO sheets was confirmed by FTIR and Raman spectroscopies. Zeta potential of the curcumin-rGO sheets (−20 mV) was found smaller than that of the GO ones (−40 mV). The curcumin-functionalized rGO sheets with concentrations <70 μg/mL showed no significant cytotoxicity and cell morphological changes. Meanwhile, they could induce further growths of cancer cells (~25% after 48 h incubation). At concentrations ≥70 μg/mL, some cytotoxic effects inducing slight cell deaths (~15–25%), cell apoptosis and cell morphological changes (from elongated to roundup morphology) were observed. These results indicated that the functionalized-rGO nanomaterials (here, curcumin-rGO) can effectively be used in nanotechnology-based bioapplications that required high concentrations of graphene, without encountering a significant toxicity.

## Acknowledgments

The authors would like to thank the Research Council of Sharif University of Technology (Grant No. G930207).

## References

[1] H.Y. Mao, S. Laurent, W. Chen, O. Akhavan, M. Imani, A.A. Ashkarran, M. Mahmoudi, Graphene: promises, facts, opportunities, and challenges in nanomedicine, Chem. Rev. 113 (2013) 3407–3424.
[2] O. Akhavan, E. Ghaderi, Toxicity of graphene and graphene oxide nanowalls against bacteria, ACS Nano 4 (2010) 5731–5736.
[3] W. Hu, C. Peng, W. Luo, M. Lv, X. Li, D. Li, et al., Graphene-based antibacterial paper, ACS Nano 4 (2010) 4317–4323.
[4] O. Akhavan, E. Ghaderi, *Escherichia coli* bacteria reduce graphene oxide to bactericidal graphene in a self-limiting manner, Carbon 50 (2012) 1853–1860.
[5] J. Ma, J. Zhang, Z. Xiong, Y. Yong, X.S. Zhao, Preparation, characterization and antibacterial properties of silver-modified graphene oxide, J. Mater. Chem. 21 (2011) 3350–3352.
[6] O. Akhavan, E. Ghaderi, Photocatalytic reduction of graphene oxide nanosheets on $TiO_2$ thin film for photoinactivation of bacteria in solar light irradiation, J. Phys. Chem. C 113 (2009) 20214–20220.
[7] O. Akhavan, M. Choobtashani, E. Ghaderi, Protein degradation and RNA efflux of viruses photocatalyzed by graphene-tungsten oxide composite under visible light irradiation, J. Phys. Chem. C 116 (2012) 9653–9659.
[8] O. Akhavan, E. Ghaderi, K. Rahimi, Adverse effects of graphene incorporated in $TiO_2$ photocatalyst on minuscule animals under solar light irradiation, J. Mater. Chem. 22 (2012) 23260–23266.
[9] N. Mohanty, V. Berry, Graphene-based single-bacterium resolution biodevice and DNA transistor: interfacing graphene derivatives with nanoscale and microscale biocomponents, Nano Lett. 8 (2008) 4469–4476.
[10] O. Akhavan, E. Ghaderi, R. Rahighi, Toward single-DNA electrochemical biosensing by graphene nanowalls, ACS Nano 6 (2012) 2904–2916.
[11] Y.Y. Shao, J. Wang, H. Wu, J. Liu, I.A. Aksay, Y.H. Lin, Graphene based electrochemical sensors and biosensors: a review, Electroanalysis 22 (2010) 1027–1036.
[12] A. Esfandiar, N.J. Kybert, E.N. Dattoli, G.H. Han, M.B. Lerner, O. Akhavan, et al., DNA-decorated graphene nanomesh for detection of chemical vapors, Appl. Phys. Lett. 103 (2013) 183110.
[13] M. Kalbacova, A. Broz, J. Kong, M. Kalbac, Graphene substrates promote adherence of human osteoblasts and mesenchymal stromal cells, Carbon 48 (2010) 4323–4329.
[14] T.R. Nayak, H. Andersen, V.S. Makam, C. Khaw, S. Bae, X. Xu, P.R. Ee, J.H. Ahn, B.H. Hong, G. Pastorin, B. Ozyilmaz, Graphene for controlled and accelerated osteogenic differentiation of human mesenchymal stem cells, ACS Nano 5 (2011) 4670–4678.
[15] O. Akhavan, E. Ghaderi, M. Shahsavar, Graphene nanogrids for selective and fast osteogenic differentiation of human mesenchymal stem cells, Carbon 59 (2013) 200–211.
[16] S.Y. Park, J. Park, S.H. Sim, M.G. Sung, K.S. Kim, B.H. Hong, S. Hong, Enhanced differentiation of human neural stem cells into neurons on graphene, Adv. Mater. 23 (2011) H263–H267.
[17] O. Akhavan, E. Ghaderi, Flash photo stimulation of human neural stem cells on graphene/$TiO_2$ heterojunction for differentiation into neurons, Nanoscale 5 (2013) 10316–10326.
[18] C. Heo, J. Yoo, S. Lee, A. Jo, S. Jung, H. Yoo, Y.H. Lee, M. Suh, The control of neural cell-to-cell interactions through non-contact electrical field stimulation using graphene electrodes, Biomaterials 32 (2011) 19–27.
[19] O. Akhavan, E. Ghaderi, Differentiation of human neural stem cells into neural networks on graphene nanogrids, J. Mater. Chem. B 1 (2013) 6291–6301.
[20] Z. Liu, J.T. Robinson, X. Sun, H. Dai, PEGylated nanographene oxide for delivery of water-insoluble cancer drugs, J. Am. Chem. Soc. 130 (2008) 10876–10877.
[21] L. Zhang, J. Xia, Q. Zhao, L. Liu, Z. Zhang, Functional graphene oxide as a nanocarrier for controlled loading and targeted delivery of mixed anticancer drugs, Small 6 (2010) 537–544.
[22] O. Akhavan, E. Ghaderi, Graphene nanomesh promises extremely efficient in-vivo photothermal therapy, Small 9 (2013) 3593–3601.
[23] K. Yang, J. Wan, S. Zhang, B. Tian, Y. Zhang, Z. Liu, The influence of surface chemistry and size of nanoscale graphene oxide on photothermal therapy of cancer using ultra-low laser power, Biomaterials 33 (2011) 2206–2214.
[24] K. Yang, L. Hu, X. Ma, S. Ye, L. Cheng, X. Shi, C. Li, Y. Li, Z. Liu, Multimodal imaging guided photothermal therapy using functionalized graphene nanosheets anchored with magnetic nanoparticles, Adv. Mater. 24 (2012) 1868–1872.
[25] O. Akhavan, A. Meidanchi, E. Ghaderi, S. Khoei, Zinc ferrite spinel-graphene in magneto-photothermal therapy of cancer, J. Mater. Chem. B 2 (2014) 3306–3314.
[26] O. Akhavan, E. Ghaderi, A. Akhavan, Size-dependent genotoxicity of graphene nanoplatelets in human stem cells, Biomaterials 33 (2012) 8017–8025.
[27] O. Akhavan, E. Ghaderi, H. Emamy, F. Akhavan, Genotoxicity of graphene nanoribbons in human mesenchymal stem cells, Carbon 54 (2013) 419–431.
[28] K. Yang, S. Zhang, G. Zhang, X. Sun, S.T. Lee, Z. Liu, Graphene in mice: ultrahigh in vivo tumor uptake and efficient photothermal therapy, Nano Lett. 10 (2010) 3318–3323.
[29] O. Akhavan, E. Ghaderi, S. Aghayee, Y. Fereydooni, A. Talebi, The use of a glucose-reduced graphene oxide suspension for photothermal cancer therapy, J. Mater. Chem. 22 (2012) 13773–13781.
[30] W. Zhang, Z. Guo, D. Huang, Z. Liu, X. Guo, H. Zhong, Synergistic effect of chemo-photothermal therapy using PEGylated graphene oxide, Biomaterials 32 (2011) 8555–8561.
[31] W. Hu, C. Peng, M. Lv, X. Li, Y. Zhang, N. Chen, C. Fan, Q. Huang, Protein corona-mediated mitigation of cytotoxicity of graphene oxide, ACS Nano 5 (2011) 3693–3700.
[32] O. Akhavan, E. Ghaderi, E. Abouei, S. Hatamie, E. Ghasemi, Accelerated differentiation of neural stem cells into neurons on ginseng-reduced graphene oxide sheets, Carbon 66 (2014) 395–406.
[33] O. Akhavan, E. Ghaderi, H. Emamy, Nontoxic concentrations of PEGylated graphene nanoribbons for selective cancer cell imaging and photothermal therapy, J. Mater. Chem. 22 (2012) 20626–20633.
[34] J. Gao, F. Liu, Y. Liu, N. Ma, Z. Wang, X. Zhang, Environment-friendly method to produce graphene that employs vitamin C and amino acid, Chem. Mater. 22 (2010) 2213–2218.
[35] A. Esfandiar, O. Akhavan, A. Irajizad, Melatonin as a powerful bio-antioxidant for reduction of graphene oxide, J. Mater. Chem. 21 (2011) 10907–10914.
[36] O. Akhavan, E. Ghaderi, A. Esfandiar, Wrapping bacteria by graphene nanosheets for isolation from environment, reactivation by sonication and inactivation by near-infrared irradiation, J. Phys. Chem. B 115 (2011) 6279–6288.
[37] O. Akhavan, M. Kalaee, Z.S. Alavi, S.M.A. Ghiasi, A. Esfandiar, Increasing the antioxidant activity of green tea polyphenols in the presence of iron for the reduction of graphene oxide, Carbon 50 (2012) 3015–3025.
[38] Y. Wang, Z.X. Shi, J. Yin, Facile synthesis of soluble graphene via a green reduction of graphene oxide in tea solution and its biocomposites, ACS Appl. Mater. Interfaces 3 (2011) 1127–1133.
[39] E. Hashemi, O. Akhavan, M. Shamsara, R. Rahighi, A. Esfandiar, A.R. Tayefeh, Cyto- and geno-toxicities of graphene oxide and reduced graphene oxide sheets on spermatozoa, RSC Adv. 4 (2014) 27213–27223.
[40] P.S. Negi, G.K. Jayaprakasha, L. Jagan Mohan Rao, K.K. Sakariah, Antibacterial activity of turmeric oil: a byproduct from curcumin manufacture, J. Agric. Food Chem. 47 (1999) 4297–4300.
[41] H. Zhou, C.S. Beevers, S. Huang, The targets of curcumin, Curr. Drug Targets 12 (2011) 332–347.
[42] D.K. Singh, R. Jagannathan, P. Khandelwal, P.M. Abraham, P. Poddar, In situ synthesis and surface functionalization of gold nanoparticles with curcumin and their antioxidant properties: an experimental and density functional theory investigation, Nanoscale 5 (2013) 1882–1893.
[43] O. Akhavan, Photocatalytic reduction of graphene oxides hybridized by ZnO nanoparticles in ethanol, Carbon 49 (2010) 11–18.
[44] H.C. Schniepp, J.L. Li, M.J. McAllister, H. Sai, M. Herrera-Alonso, D.H. Adamson, et al., Functionalized single graphene sheets derived from splitting graphite oxide, J. Phys. Chem. B 110 (2006) 8535–8539.

[45] M.J. McAllister, J.L. Li, D.H. Adamson, H.C. Schniepp, A.A. Abdala, J. Liu, et al., Single sheet functionalized graphene by oxidation and thermal expansion of graphite, Chem. Mater. 19 (2007) 4396–4404.
[46] O. Akhavan, The effect of heat treatment on formation of graphene thin films from graphene oxide nanosheets, Carbon 48 (2010) 509–519.
[47] O. Akhavan, K. Bijanzad, A. Mirsepah, Synthesis of graphene from natural and industrial carbonaceous wastes, RSC Adv. 4 (2014) 20441–20448.
[48] Q. Su, S. Pang, V. Alijani, C. Li, X. Feng, K. Müllen, Composites of graphene with large aromatic molecules, Adv. Mater. 21 (2009) 3191–3195.
[49] A. Meidanchi, O. Akhavan, Superparamagnetic zinc ferrite spinel–graphene nanostructures for fast wastewater purification, Carbon 69 (2014) 230–238.
[50] O. Akhavan, M. Abdolahad, A. Esfandiar, M. Mohatashamifar, Photodegradation of graphene oxide sheets by $TiO_2$ nanoparticles after a photocatalytic reduction, J. Phys. Chem. C 114 (2010) 12955–12959.
[51] G. Eda, Y.Y. Lin, C. Mattevi, H. Yamaguchi, H.A. Chen, I.S. Chen, C.W. Chen, M. Chhowalla, Blue photoluminescence from chemically derived graphene oxide, Adv. Mater. 22 (2010) 505–509.
[52] Z. Luo, Y. Lu, L.A. Somers, A.T.C. Johnson, High yield preparation of macroscopic graphene oxide membranes, J. Am. Chem. Soc. 131 (2009) 898–899.
[53] S. Hatamie, M. Nouri, S.K. Karandikar, A. Kulkarni, S.D. Dhole, D.M. Phase, S.N. Kale, Complexes of cobalt nanoparticles and polyfunctionalcurcumin as antimicrobial agents, Mater. Sci. Eng. C 32 (2012) 92–97.
[54] F. Tuinstra, J.L. Koenig, Raman spectrum of graphite, J. Chem. Phys. 53 (1970) 1126–1130.
[55] A.C. Ferrari, J. Robertson, Interpretation of Raman spectra of disordered and amorphous carbon, Phys. Rev. B 61 (2000) 14095–14107.
[56] K.N. Kudin, B. Ozbas, H.C. Schniepp, R.K. Prud'homme, I.A. Aksay, R. Car, Raman spectra of graphite oxide and functionalized graphene sheets, Nano Lett 8 (2008) 36–41.
[57] O. Akhavan, Graphene nanomesh by ZnO nanorod photocatalysts, ACS Nano 4 (2010) 4174–4180.
[58] A. Dato, V. Radmilovic, Z. Lee, J. Phillips, M. Frenkach, Substrate free gas-phase synthesis of graphene sheets, Nano Lett. 8 (2008) 2012–2016.
[59] A.C. Ferrari, J.C. Meyer, V. Scardaci, C. Casiraghi, M. Lazzeri, F. Mauri, et al., The Raman fingerprint of graphene and graphene layers, Phys. Rev. Lett. 97 (2006) 187401.
[60] L.M. Malard, M.A. Pimenta, G. Dresselhaus, M.S. Dresselhaus, Raman spectroscopy in graphene, Phys. Rep. 473 (2009) 51–87.
[61] D. Graf, F. Molitor, K. Ensslin, C. Stampfer, A. Jungen, C. Hierold, et al., Spatially resolved Raman spectroscopy of single- and few-layer graphene, Nano Lett. 7 (2007) 238–242.
[62] K.S. Kim, Y. Zhao, H. Jang, S.Y. Lee, J.M. Kim, K.S. Kim, et al., Large-scale pattern growth of graphene films for stretchable transparent electrodes, Nature 457 (2009) 706–710.
[63] I. Calizo, A.A. Balandin, W. Bao, F. Miao, C.N. Lau, Temperature dependence of the Raman spectra of graphene and graphene multilayers, Nano Lett. 7 (2007) 2645–2649.
[64] L. Liu, S. Ryu, M.R. Tomasik, E. Stolyarova, N. Jung, M.S. Hybertsen, et al., Graphene oxidation: thickness-dependent etching and strong chemical doping, Nano Lett. 8 (2008) 1965–1970.
[65] H. Schulz, M. Baranska, Identification and quantification of valuable plant substances by IR and Raman spectroscopy, Vib. Spectrosc. 43 (2007) 13–25.
[66] T.M. Kolev, E.A. Velcheva, B.A. Tamboliyska, M. Spiteller, DFT and experimental studies of the structure and vibrational spectra of curcumin, Int. J. Quantum Chem. 102 (2005) 1069–1079.
[67] Y. Xu, Z. Liu, X. Zhang, Y. Wang, J. Tian, Y. Huang, Y. Ma, X. Zhang, Y. Chen, A graphene hybrid material covalently functionalized with porphyrin: synthesis and optical limiting property, Adv. Mater. 21 (2009) 1275–1279.
[68] C. Shan, H. Yang, D. Han, Q. Zhang, A. Ivaska, L. Niu, Water-soluble graphene covalently functionalized by biocompatible poly-L-lysine, Langmuir 25 (2009) 12030–12033.
[69] J. Shen, M. Shi, B. Yan, H. Ma, N. Li, Y. Hu, M. Ye, Covalent attaching protein to graphene oxide via diimide-activated amidation, Colloids Surf. B 81 (2010) 434–438.
[70] D. Pan, J. Zhang, Z. Li, M. Wu, Hydrothermal route for cutting graphene sheets into blue-luminescent graphene quantum dots, Adv. Mater. 22 (2010) 734–738.
[71] X. Sun, Z. Liu, K. Welsher, J.T. Robinson, A. Goodwin, S. Zaric, H. Dai, Nano-graphene oxide for cellular imaging and drug delivery, Nano Res. 1 (2008) 203–212.
[72] G. Wang, J. Yang, J. Park, X. Gou, B. Wang, H. Liu, J. Yao, Facile synthesis and characterization of graphene nanosheets, J. Phys. Chem. C 112 (2008) 8192–8195.
[73] E.E. Ghadim, N. Rashidi, S. Kimiagar, O. Akhavan, F. Manouchehri, E. Ghaderi, Pulsed laser irradiation for environment friendly reduction of graphene oxide suspensions, Appl. Surf. Sci. 301 (2014) 183–188.
[74] O. Akhavan, E. Ghaderi, The use of graphene in the self-organized differentiation of human neural stem cells into neurons under pulsed laser stimulation, J. Mater. Chem. B 2 (2014) 5602–5611.
[75] F. Liu, T.S. Seo, A controllable self-assembly method for large-scale synthesis of graphene sponges and free-standing graphene films, Adv. Funct. Mater. 20 (2010) 1–7.
[76] R.R. Arivizo, O.R. Miranda, M.A. Thompson, C.M. Pabelick, R. Bhattacharya, J.D. Robertson, V.M. Rotello, Y.S. Prakash, P. Mukherjee, Nano Lett. 10 (2010) 2543–2548.
[77] Y. Fazaeli, O. Akhavan, R. Rahighi, M.R. Aboudzadeh, E. Karimi, H. Afarideh, In vivo SPECT imaging of tumors by $^{198, 199}$Au-labeled graphene oxide nanostructures, Mater. Sci. Eng. C 45 (2014) 196–204.